Polymer-Stabilized Cholesteric Diffraction Gratings: Effects of UV Wavelength on Polymer Morphology and Electrooptic Properties

Shin-Woong Kang,*,† Samuel Sprunt,‡ and Liang-Chi Chien†

Chemical Physics Interdisciplinary Program and Liquid Crystal Institute and Department of Physics, Kent State University, Kent Ohio, 44242

Received March 28, 2006. Revised Manuscript Received July 10, 2006

We compare the performance of polymer-stabilized cholesteric liquid crystal diffraction gratings for two limits of the polymer morphology: a one-dimensional array of polymer walls that extend through the grating thickness ("bulk network"), and a thin layer of patterned polymer fibrils localized at one surface ("surface network"). In each case, the polymer is spatially templated by the liquid crystal orientational order, but the depth of the network is dictated by UV absorbance of the liquid crystal and a choice of wavelength used to initiate photopolymerization. Whereas both polymer morphologies yield robust electrically switchable gratings, the surface-stabilized grating operates at lower field thresholds and shorter transition times. However, the patterning of the surface network significantly reduces the contrast between grating on and off states, a limitation that can be potentially offset by employing isotropic monomers index-matched to the liquid crystal.

Introduction

Switchable optical diffraction gratings play a central role in current technologies such as multiplexing and processing optical signals (optical interconnection, beam steering, and sensor array interrogation).[1−3] Combined with various external tools to induce or modify distinct, spatially periodic variations in orientational order, liquid crystals can be used to produce efficient transmission/reflection phase gratings with the competitive advantages of low cost and weight and high processibility for large-area formats.[3] The optical properties of liquid crystals exhibit a large bulk response to low applied voltages or fields, making large-format LC gratings dynamically adjustable with low power consumption, a particular advantage over inorganic materials. This responsiveness, combined with fluidity and rational control over dielectric/optical anisotropy, chirality, and optical pitch through organic synthesis, allows for the convenient tuning of key grating properties over a wide range.

Several alternative approaches for liquid crystal gratings have been investigated. These involve either the use of a patterned alignment layer (or electrode) on a substrate supporting a low-molecular-weight liquid crystal, an approach that produces domains of alternating orientation of the LC optic axis,[4−7] or the use of polymer−liquid crystal composites, where a light controlled polymer−liquid crystal phase separation produces an internal grating structure.[8−12] In such systems, a refractive index gradient is imposed by lithographically (or holographically) patterning the alignment layer/electrode or distribution of liquid crystal droplets with a random average director orientation within a polymer binder. A more recent alternative is the polymer-stabilized cholesteric liquid crystal diffraction grating (PSCDG).[13,14] Here, the grating is formed by stabilizing, via UV-induced photopolymerization of a low-volume fraction polymer network, the light-diffracting fingerprint state of a cholesteric LC, which is induced in a standard electrooptical cell by an applied electric field. The resulting grating can function in either the Bragg or Raman−Nath (phase grating) limits[15−17]

* To whom correspondence should be addressed.E-mail: skang1@kent.edu.
† Chemical Physics Interdisciplinary Program and Liquid Crystal Institute, Kent State University.
‡ Department of Physics, Kent State University.

(1) (a) Sutherland, R. L.; Tondiglia, V. P.; Natarajan, L. V.; Bunning, T. J.; Adams, W. W. *Appl. Phys. Lett.* **1994**, *64*, 1074. (b) Gibbons, W. M.; Sun, S.-T. *Appl. Phys. Lett.* **1994**, *65*, 2542.
(2) Gupta, V. K.; Abbott, N. L. *Science* **1997**, *276*, 1533.
(3) (a) Domash, L.; Gozewski, C.; Nelson, A.; Schwartz, J. *Proc. SPIE* **1993**, *2026*, 642. (b) McManamon, P. F.; et al. *Proc. IEEE* **1996**, *84*, 268. (c) Nelson, A. R.; Chen, T.; Jauniskis, L.; Domash, L. H. *Proc. SPIE* **1995**, *2404*, 182. (d) Domash, L.; Haugsjaa, P.; Little, B. E. *Proc. SPIE* **1998**, *3234*, 1. (e) Kanto, K.; Hisaki, T.; Date, M.; Nakajima, H. Proc. *SPIE* **1998**, *3297*, 52. (f) Takahashi, N.; Yoshimura, K.; Takahashi, S.; Imamura, K. *IEICE Trans. Electron.* **2000**, *E83-C*, 275.
(4) Chen, J.; Bos, P. J.; Vithana, H.; Johnson, D. L. *Appl. Phys. Lett.* **1995**, *67*, 2588.
(5) Titus, C. M.; Bos, P. J. *Appl. Phys. Lett.* **1997**, *71*, 2239.
(6) Fukushima, S.; Kurokawa, T. *Jpn. J. Appl. Phys.* **1994**, *33*, 5747.
(7) He, Z.; Nose, T.; Sato, S. *Jpn. J. Appl. Phys.* **1996**, *35*, 3529.
(8) (a) Sutherland, R. L.; Natarajan, L. V.; Tondiglia, V. P. *Chem. Mater.* **1993**, *5*, 1533. (b) Natarajan, L. V.; Shepherd, C. K.; Brandelik, D. M.; Sutherland, R. L.; Chandra, S.; Tondiglia, V. P.; Tomlin, D.; Bunning, T. J. *Chem. Mater.* **2003**, *15*, 2477. (c) Bunning, T. J.; Kirkpatrick, S. M.; Natarajan, L. V.; Tondiglia, V. P.; Tomlin, D. W. *Chem. Mater.* **2000**, *12*, 2842.
(9) (a) Bowley, C. C.; Crawford, G. P. *Appl. Phys. Lett.* **2000**, *76*, 2235. (b) Kossyrev, P. A.; Crawford, G. P. *Appl. Phys. Lett.* **2001**, *79*, 296.
(10) (a) Fuh, A. Y.-G.; Tsai, M.-S.; Huang, C.-Y.; Ko, T.-C.; Chien, L.-C. *Opt. Quantum Electron.* **1996**, *28*, 1535. (b) Fuh, A. Y.-G.; Tsai, M.-S.; Huang, C.-Y.; Ko, T.-C.; Chien, L.-C. *J. Appl. Phys.* **1998**, *83*, 679.
(11) Cipparrone, G.; Mazzulla, A.; Nicoletta, F. P.; Lucchetti, L.; Simoni, F. *Opt. Commun.* **1998**, *150*, 297.
(12) Cipparrone, G.; Muzzulla, A.; Russo, G. *Appl. Phys. Lett.* **2001**, *78*, 1186.
(13) Lee, S. N.; Chien, L. C.; Sprunt, S. *Appl. Phys. Lett.* **1998**, *72*, 885.
(14) (a) Kang, S. W.; Sprunt, S.; Chien, L. C. *Appl. Phys. Lett.* **2000**, *76*, 3516. (b) Kang, S. W.; Sprunt, S.; Chien, L. C. *Appl. Phys. Lett.* **2001**, *78*, 3782.

10.1021/cm060734w CCC: $33.50 © 2006 American Chemical Society
Published on Web 08/15/2006

and exhibits an ~10−100 ms on/off response to reasonably low applied electric fields. However, the specific morphology of the polymer network and its precise connection to the control and optimization of the electrooptical properties of the composite system remain largely unexplored.

In this report, we investigate the nature and effect on optical response of variation in the polymer morphology for two distinct limits of the wavelength of UV radiation used in the photopolymerization process.[18,19] In the short wavelength, high absorption limit, a patterned surface network is formed, which stabilizes a diffraction grating switchable at one-half to one-third the electric field required for bulk-stabilized gratings produced by longer wavelength UV irradiation. The off state obtainable in the surface-stabilized grating is limited by the LC templated patterning of the thin surface layer of polymer, which produces significant residual diffraction even when the bulk LC is switched to the uniform (nondiffracting) state. This effect is almost absent in the case of bulk stabilization because of better index-matching between LC and patterned polymer fibrils that have a normal-to-substrate orientation characteristic of the bulk morphology. The dynamics of the electrooptic response are notably different between the two cases; the bulk-stabilized grating exhibits two distinct time scales corresponding to coupled fast LC and slow polymer motion, whereas the dynamic response is almost completely dominated by the LC component in the surface-stabilized grating.

Experimental Section

The materials used are listed in the Supporting Information. Figure S1 in the Supporting Information illustrates a process for the preparation of PSCDGs. A uniform fingerprint texture (b) was obtained from the initial π-twisted planar state (a) under an applied electric field $E = 0.25$ V/μm. This reversibly transforms to the initial planar or homeotropic states (c) at a higher field value $E = 0.41$ V/μm. The stabilization of the grating texture is accomplished by the photopolymerization of ~5 wt % reactive monomer, included in the initial mixture of components. The resulting light-diffracting state (d) is then stable against removal of the field. The zero-field diffraction grating can be reproducibly tuned to other diffracting states or switched off to a nondiffracting state (e) by suitably varying an applied electric field.

Fixed 5 wt % reactive monomer (RM 257, Merck), 0.4 wt % chiral dopant (R1011, Merck), and 0.2 wt % photoinitiator (Iragcure 651, Ciba additives) were dissolved in a nematic LC host (BL 006, Merck). The homogeneous mixture was then moved into standard electrooptic cells by capillary action at room temperature. The electrooptic cells consisted of indium−tin oxide coated conductive glass substrates with a uniform gap of 10 ± 0.5 μm. For a homogeneous LC alignment, the inner surfaces of the substrates were coated with polyimide alignment layers, which were uniaxially rubbed and assembled at a 180° angle with respect to each rubbing direction, over transparent electrodes.

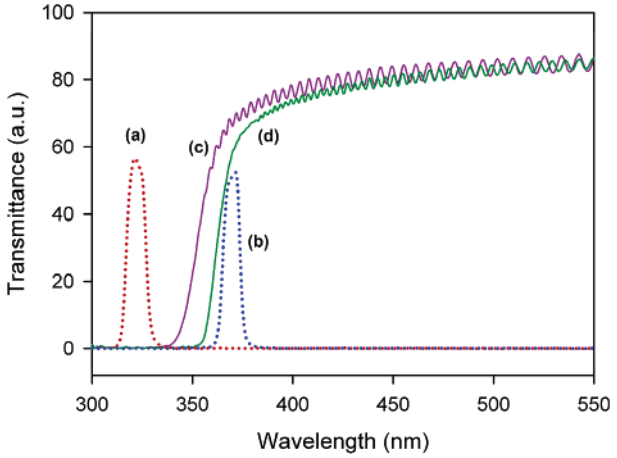

Figure 1. UV−vis spectra of the LC cell and band-pass filters. (a) and (b) represent the pass band for the 322 and 365 nm filters, respectively, used for polymer stabilization. The incident light is polarized (c) perpendicular and (d) parallel to the director of a homogeneously aligned nematic LC.

In the initial planar state at zero field, the director twists from the bottom to the top of the substrate, with the axis of twist perpendicular to the substrate plane. A square wave voltage (0.31 V/μm across the 10 μm cell thickness at 1 kHz) was then applied to form a planar grating (fingerprint) texture, which appears in the polarizing microscope as a uniform pattern of stripes. The electric field distorts and reorients the cholesteric helix into the substrate plane, with the "helical" axis running perpendicular to the rub direction (and to the stripes). In general, the slower formation of the grating texture using a weaker electric field results in more uniform textures in a macroscopic scale. The spatial period or pitch of the grating texture can be controlled by the concentration of a chiral dopant. With the magnitude of the electric field kept constant at 0.41 V/μm for a better defined diffraction pattern, the grating texture was stabilized by polymerizing the reactive monomer using collimated UV irradiation (Oriel 6258 with a 150 W xenon lamp) for 30 min. Two wavelengths, 322 and 365 nm, were selected by band-pass filters. The intensity of the incident UV to the cell was kept at 0.04 mW/cm^2 for 365 nm and 0.08 mW/cm^2 for 322 nm. The higher intensity for the 322 nm wavelength was to compensate for a factor of 2 higher absorption by the substrate. The intensity level was measured at the sample position using a light intensity controller system (Oriel 68850). Figure 1 shows the UV−vis transmittance of the loaded LC cell for polarization perpendicular (curve c) and parallel (curve d) to a uniform, homogeneously aligned director as well as the pass band for the two filters used (curves a and b). Clearly, the complete cell transmits ~70% at 365 nm, whereas the 322 nm light is strongly absorbed by the LC layer.

A schematic diagram of the experimental setup used for characterizing diffraction properties is presented in Figure S2 (see the Supporting Information). The diffraction patterns of samples were recorded using normally incident He−Ne laser light and a charge-coupled-device (CCD) detector. The He−Ne beam was polarized perpendicular to the grating axis for maximum grating contrast. No analyzer was used. The polarization of the incident light was controlled using a halfwave (λ/2) plate placed in front of the sample. The recorded CCD image was used to obtain the

(15) (a) Sackmann, E.; Meiboom, S.; Synder, L. C.; Mexner, A. E.; Dietz, R. E. *J. Am. Chem. Soc.* **1968**, *90*, 3567. (b) Soffer, B. H.; et al. *Mol. Cryst. Liq. Cryst.* **1981**, *70*, 145. (c) Suresh, K. A.; Kumar, P. B. S.; Ranganath, G. S. *Liq. Cryst.* **1992**, *11*, 73.
(16) Subacius, D.; Bos, P. J.; Lavrentovich, O. D. *Appl. Phys. Lett.* **1997**, *71*, 1350.
(17) (a) Subacius, D.; Shiyanovski, S. V.; Bos, P. J.; Lavrentovich, O. D. *Appl. Phys. Lett.* **1997**, *71*, 3323. (b) Lavrentovich, O. D.; Subacius, D.; Shiyanovski, S. V.; Bos, P. J. *SPIE* **1998**, *3292*, 37.
(18) Other approaches have been developed to produce surface-localized polymer structure in liquid crystal hosts in order to enhance the performance of electrooptic displays and reflectors. However, these methods did not utilize the wavelength of the UV selectively. (a) Vorflusev, V.; Kumar, S. *Science* **1999**, *283*, 1903. (b) Broer, D. J.; Lub, J.; Mol, G. N. *Nature* **1995**, *378*, 467.
(19) (a) Kang, S. W.; Sprunt, S.; Chien, L. C. *Adv. Mater.* **2001**, *13*, 1179. (b) Kang, S. W.; Sprunt, S.; Chien, L. C. *Polym. Prepr.* **2001**, *42* (2), 581. (c) Kang, S. W.; Sprunt, S.; Chien, L. C. *Mater. Res. Soc. Symp. Proc.* **2002**, *709*, CC6.3.1.

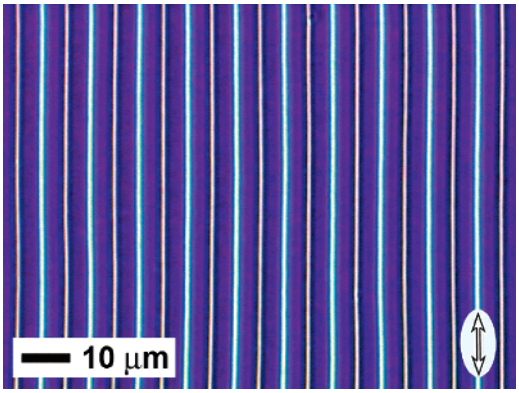

Figure 2. Polarized optical micrograph of the cholesteric diffraction grating prior to polymerization. The texture was obtained by applying a square waveform electric field (0.41 V/μm, 1 kHz). The double-ended arrow represents the surface rub direction.

intensity profile for diffracted light. This multiple-peak intensity profile was fitted using a Gaussian function (the commercial software, Peak Fit 4.0). The relative intensity of each diffracted peak was calculated by integrating the area of fitted peaks and used to calculate the diffraction efficiency of the sample. The diffraction efficiency, in this study, was defined as the ratio of the diffracted light intensity to the total light intensity in all orders. The absorption and scattering losses are not considered. To measure the dynamic response, the undiffracted (zero-order) light intensity was monitored using an oscilloscope and a silicon photodetector (10 MHz bandwidth) operated in photovoltaic mode. The amplitude-modulated square wave electric field was applied to the sample at a frequency of 1 kHz with a 1−10 Hz modulation frequency. The resulting oscilloscope traces were saved as a data file and plotted using spreadsheet type software.

For polarizing optical microscopy (POM) and scanning electron microscopy (SEM) imaging of the polymer network, a 70/30 mixture of hexane and dichloromethane was used to dissolve out preferentially the LC from the stabilized samples. The optical texture of the bare network was then examined using a Nikon OPTIPHOT2-POL microscope. The cells were then carefully opened, and a thin gold layer was deposited on the inner surface. The polymer morphology was observed using a JEOL JSM-6300V scanning electron microscope operated at 10 kV in the secondary electron imaging mode.

Results and Discussion

Figure 2 shows a typical microscope image (taken through crossed polarizers) of the electric field-induced fingerprint texture of the cholesteric mixture prior to polymer stabilization. After polymerization and removal of the field, the optical texture is maintained and is essentially indistinguishable for the two different UV polymerization conditions (322 and 365 nm wavelengths) used. After evacuation of the LC, the optical textures of the bare polymer networks (Figure 3) both show a one-dimensional patterning that is clearly templated on the periodic variation in orientational order of the LC host characteristic of the fingerprint state. Rotating the samples between crossed polarizers confirms that the patterned polymer domains are bi-refringent, indicating significant orientational order impressed on the polymer network by the host. For the sample stabilized by 365 nm UV light (Figure 3a), the polymer domains are spaced with a 5 μm period; however, one can see from the variation in

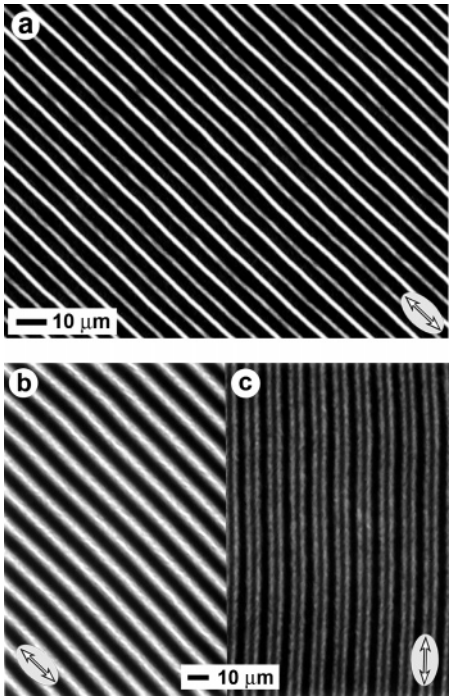

Figure 3. Polarized optical micrographs of the templated polymer patterns after polymerization of a reactive monomer in the grating texture and subsequent removal of LCs: (a) polymerized using 365 nm and (b,c) 322 nm band-pass filters, respectively. Polarizer and analyzer are parallel and perpendicular to the figure. The double-ended arrows represent the surface rub direction.

intensity and color between adjacent stripes that the complete polymer structure is apparently formed by the interdigitation of two separate sets of 10 μm spaced domains, which are shifted by 5 μm with respect to each other.

The optical texture of the network formed with 322 nm UV radiation (substantially absorbed by the host LC) exhibits a broader one-dimensional pattern with a 10 μm period when stripes are aligned 45° to the polarizers (Figure 3b). Upon rotation of the sample in the substrate plane, the bright lines turn dark and dark lines become bright with a narrow dark stripe through the center, as shown in Figure 3c. When the stripes are oriented parallel to the polarizer, an interdigitated pattern consisting of two distinct stripes with a 10 μm period is clearly seen. This result indicates that the orientational order of the polymer varies spatially in a more complex fashion than in the case where deeply penetrating (365 nm) UV radiation was used. We can infer that this greater complexity results from different templating conditions in the region near the rubbed substrate surface (compared to the average through the bulk) and from the strong localization effect due to absorption of the short-wavelength UV light.

As demonstrated in Figure 4, the network morphologies examined by the SEM are strikingly distinct for different wavelengths of UV radiation. For 365 nm UV, the bulk network was templated throughout the entire sample thickness (Figure 4a). The SEM image demonstrates very thin but dense vertical walls made up of fine polymer fibrils. Very regularly spaced polymer walls with a 10 μm period are observed on opposing surfaces of the two substrates after pulling apart the cell. To obtain the same pattern observed by optical microscopy, we can deduce that the polymer walls anchored on opposite substrates are simply interdigitated.

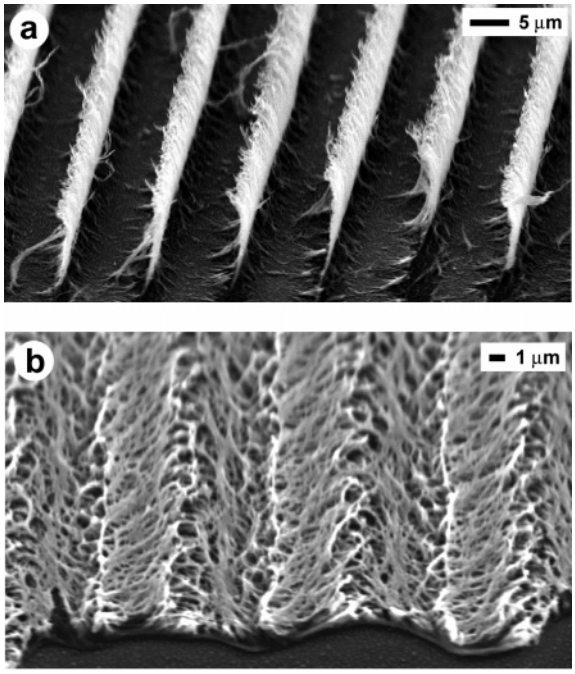

Figure 4. SEM micrographs of the network morphologies templated on the grating texture using (a) 365 and (b) 322 nm UV light for the polymerization. In (a), note the vertical-to-substrate fibril morphology within the polymer wall structure, whose regular spacing is based on the pitch of the "fingerprint" state of the host liquid crystal. This contrasts with the mostly planar (but spatially varying) fibril orientation of the surface-localized network in (b). The wide view version of images (Figure S3) is available in the Supporting Information.

In contrast, for 322 nm UV, the network was entirely localized into a thin layer (~1 μm thickness) on the substrate nearest the UV light (Figure 4b). No network formation is observed on the opposite substrate. In this case, the UV light is strongly absorbed by the host LC, and a large intensity gradient exists along the light propagation direction normal to the substrate. Therefore, the selective photoinitiation of polymerization and consequent monomer diffusion form a strongly surface-localized network.[18,19] The optical pattern (or anisotropy) of polymer reflects the orientational order (or director profile) of the host LC near the surface. As shown in Figure 4b, the polymer fibrils form a one-dimensional array consisting of four different orientations of optic axis in one period within the substrate plane.

The diffraction properties of PSCDGs formed from the cholesteric fingerprint textures are sensitive to the polarization of the incident laser light. The gratings show the maximum and minimum diffraction efficiency for the incident-light polarization perpendicular and parallel to the grating axis, respectively. The optical diffraction pattern after stabilization consisted of many orders of diffracted spots with complicated intensity distribution, suggesting that the optical profile is determined by a combination of a distorted cholesteric helix and a spatial variation in the dielectric properties of the network itself. Diffraction orders corresponding to harmonics of the optical periodicity $P = 5$ μm (observed in microscope images of Figures 2−4) are labeled with integers. In addition, half-integer peaks, corresponding to a period $2P = 10$ μm associated with the spacing of polymer domains on separate substrates, are observed with a much lower intensity.

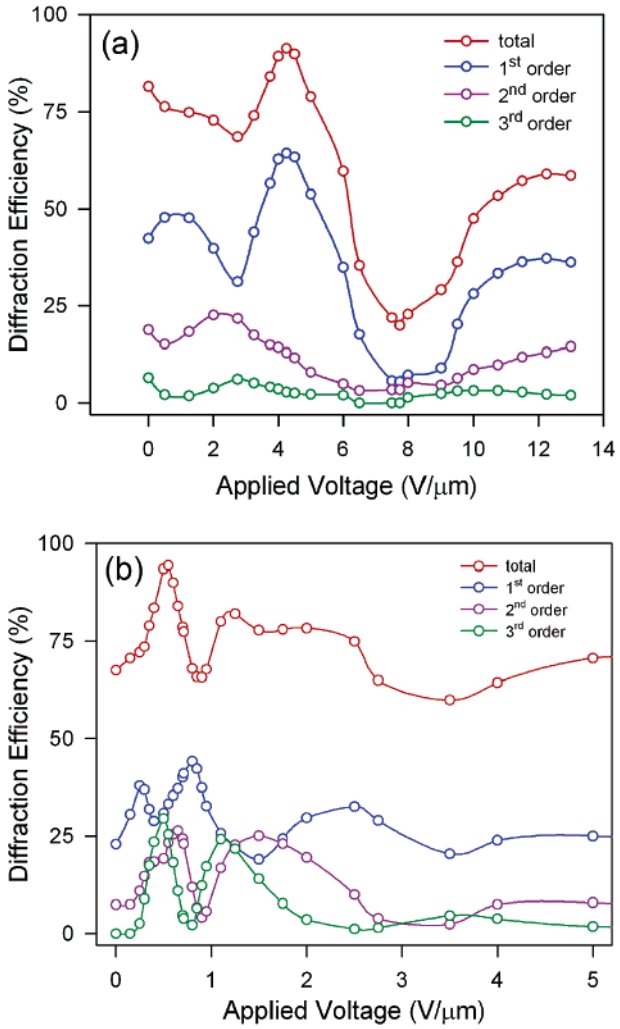

Figure 5. Applied electric field dependence of diffraction efficiencies for the samples stabilized by (a) the bulk network (b) the surface-localized network, formed using 365 and 322 nm UV radiation, respectively.

The morphological difference between surface and bulk polymer networks leads to a significant variation in the electrooptic performance of PSCDGs. The applied field dependence of the diffraction efficiency for the samples with bulk- (365 nm UV radiation) and surface-localized (322 nm UV) networks is presented in panels a and b, respectively, of Figure 5. The most striking difference is the operating electric field of the grating. The grating stabilized by the surface network exhibits a significantly lower field response because of the small internal surface for anchoring the liquid crystal (for example, the best obtainable grating off state occurs at approximately 3.5 V/μm). By contrast, the bulk network provides a relatively large internal surface, and consequently, severely inhibits the response of LC to the applied field (the grating off state corresponds to 8.3 V/μm). For the surface-stabilized grating, the applied fields less than 2 V/μm are sufficient to shift the diffracted light intensity among different orders (Figures 5b and 6a−c). However, for these gratings, planar variation of the polymer fibril orientation in the thin surface layer (Figure 4b) contributes to a poor grating-off state (Figures 5b and 6c). Note that this is quite different from the effect of the bulk morphology, Figure 4a, where the fibril orientation is mostly vertical to the substrate and constant across it. In this case, when the

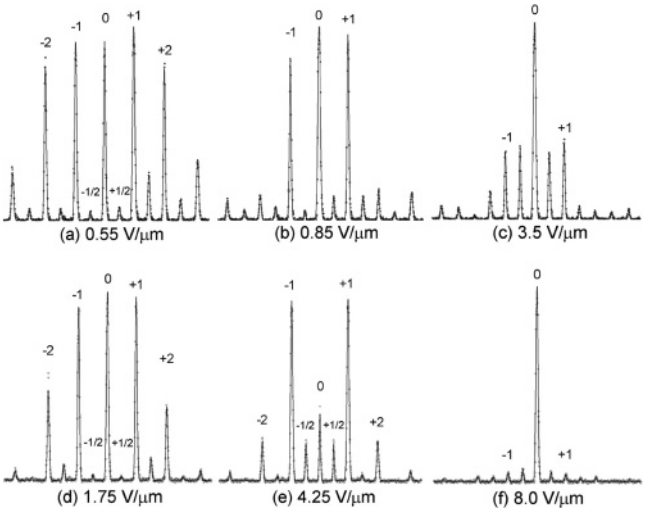

Figure 6. Transmitted light intensity profiles at different applied field levels obtained from the gratings stabilized by (a−c) the surface-localized and (d−f) the bulk networks, formed using 322 and 365 nm UV radiation, respectively. The peaks labeled by integers and half-integers correspond to the grating period $P = 5$ μm and $2P = 10$ μm, respectively.

LC is switched into a uniform orientation with the optic axis perpendicular to the substrates (parallel to the bulk fibril orientation), the phase contrast across the grating is greatly reduced, resulting in a good off state. Figure 6 presents representative far-field diffraction patterns, as a function of the applied field, obtained with normally incident 633 nm laser light polarized perpendicular to the grating axis. These data show the sensitive response of PSCDG gratings (note the dramatic shifts in intensity among diffraction orders).

To overcome the limitation of residual diffraction in the grating off state for the surface-stabilized configuration, one could use a nonmesogenic monomer with no inherent optical anisotropy and also reduce the monomer concentration in the initial mixture to the minimum required for stabilizing the LC grating. (It is well-established[14] that polymer networks formed from a low concentration of isotropic monomer are also efficient in stabilizing different states of LC orientational order.) A schematic illustrating the potential advantage of using isotropic monomers is shown in Figure 7. In the top panel, regular variation of fibril orientation corresponds to rotation of the optic axis of the mesogenic monomer and produces strong refractive index contrast ($n_{p1}-n_{p4}$) between neighboring domains. The bottom panel indicates how, using monomers that form isotropic domains in the host LC, one can produce a polymer layer with nearly uniform index (n_p). If this is then matched with the ordinary index of the LC ($n_o \approx n_p$), one should obtain a high-quality grating off state.

As revealed in Figure 8, the dynamic switching behavior of the gratings is also dramatically different for the surface versus bulk stabilization. In general, one expects the relaxation in PSCDGs from grating off to on states after reduction of the applied field to contain both fast (LC-dominated) and slow (network-dominated) components, because of the alternation of polymer-rich and -poor domains. This is, indeed, clearly the case for the bulk-stabilized grating (Figure 8b), where a fast <10 ms relaxation is followed by a much slower (≫100 ms) decay in the zero-order (undiffracted) intensity. The sample with a surface network (Figure 8a),

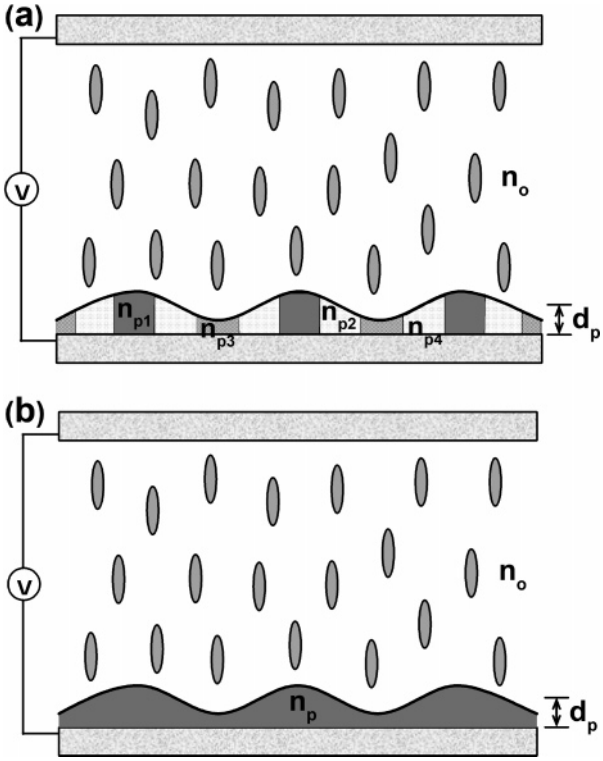

Figure 7. Schematic representation of surface-localized networks with (a) patterned and (b) uniform refractive indices, which could be formed using mesogenic and nonmesogenic reactive monomers, respectively.

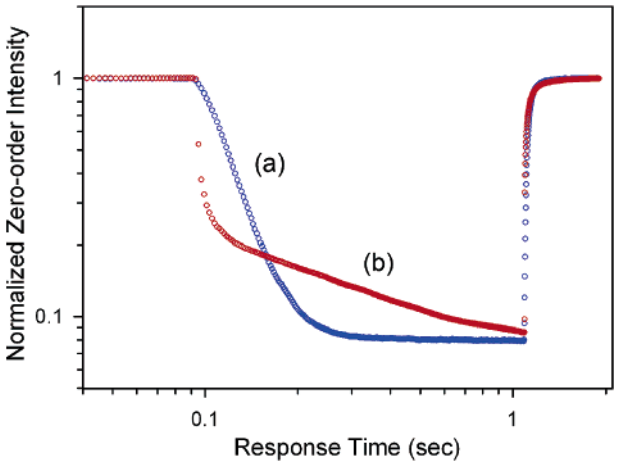

Figure 8. Log−log plot of the dynamic switching behaviors of the gratings stabilized by (a) the surface network and (b) the bulk network.

however, exhibits no bifurcation in its relaxation between grating off (higher applied field) and on (low field) states; the characteristic decay time (∼100 ms) is consistent with relaxation of pure LC from the uniform vertical to fingerprint orientational states. This is expected, because the surface network is effectively decoupled from reorientations in the LC bulk that take place along axes parallel to the substrates. However, it is interesting that at short times, the off state decays more rapidly after field removal in the bulk-stabilized sample. Without knowing the details of the spatial distribution of the LC optic axis, it is not clear whether we should attribute this to a nonlinear relaxation from a highly distorted state or to a fast switching interfacial layer of LC running along the polymer walls across the thickness of the sample.

To conclude, let us summarize how the polymer network enhances the basic potential of utilizing complex pattern-forming states in liquid crystals for optical beam steering and switching applications. In general, the polymer component internally stabilizes a particular optical state or texture of the liquid crystal, and thereby plays a critical role in both realizing and enhancing the performance of each device. In this context, the polymer microstructure serves several important purposes. First, as demonstrated in previous work on one-dimensional gratings,[13,14] it can be used to stabilize the grating structure against removal of the electric field originally required to induce the diffracting state. This stabilization has a crucial advantage over nonstabilized cholesteric gratings[15−17] for practical device applications, because formation of defect-free planar grating texture in cholesterics typically requires slow nucleation and growth followed by the annealing of defects in an applied field. Once the texture is stabilized, however, no defect formation or annealing is involved in the electrooptical response, so that polymer stabilization facilitates relatively fast switching between diffracting and nondiffracting states. In this case, the network also provides an internal "memory" for the diffracting states, ensuring reproducibility of the spatial pattern of diffracted spots when the field is cycled between states. Second, the network itself provides a one-time adjustable degree of optical contrast in the grating. This can be used to optically compensate the grating state of the LC or can be combined with electric-field tuning of the orientational profile of the LC to achieve a wider range of diffracted intensity profiles (on the basis of a fixed pitch). Third, the patterned, low-volume network significantly lowers operating voltages or fields compared to other, more concentrated polymer-containing LC devices. In general, distributed polymer networks increase switching voltage because of strong anchoring effects on the LC. Yet, in the case of a spatially segregated network[19] (that still achieves an overall purpose of anchoring a particular LC state), the LC molecules are nearly as free to respond as they would be in a completely low-molecular-weight environment. This is particularly true in the case of a surface-localized network, as we have described in this work.

In this work, we have compared the electrooptic performance of PSCDGs stabilized by bulk and surface-localized polymer networks. At present, the relative speed and low operating electric field advantages of the surface-stabilized LC gratings are somewhat offset by a more limited dynamic range and contrast between diffracting states, due mainly to background diffraction arising from the patterned polymer layer. However, it seems reasonably clear that this tradeoff can be removed, and the advantages further enhanced, by combining a suitable selection or synthesis of optically isotropic monomers with a rational choice of the LC and with careful performance simulations based on currently available computer software[20,21] that models the distorted LC states and the light diffraction arising from them.

Supporting Information Available: Material information, schematic illustration of the sample preparation of PSCDGs, experimental setup used for diffraction measurements, SEM images viewed from normal to the substrate in wide area. This material is available free of charge via the Internet at http://pubs.acs.org.

CM060734W

(20) *Defects in Liquid Crystals: Computer Simulations, Theory and Experiments*; Lavrentovich, O. D., Pasini, P., Zannoni, C., Zumer, S., Eds.; Kluwer Academic: Dordrecht, The Netherlands, 2001; pp 229−270 and references therein.

(21) Oswald, P.; Pieranski, P. *Nematic and Cholesteric Liquid Crystals*; Taylor & Francis: Oxford, U.K., 2005; Chapter VII and references therein.